MATHEMATICAL MODELING AND COMPUTING, Vol. 10, No. 4, pp. 1230–1238 (2023)

Derivation of hyper-singular integral equations for thermoelectric bonded materials featuring a crack parallel to interface

Mohd Nordin M. H. I.[1], Hamzah K. B.[2,3], Khashiie N. S.[2,3], Waini I.[2,3], Zainal N. A.[2,3], Sayed Nordin S. K.[2,3]

[1] *Fakulti Kejuruteraan Pembuatan, Universiti Teknikal Malaysia Melaka, Hang Tuah Jaya, 76100 Durian Tunggal, Melaka, Malaysia*
[2] *Fakulti Teknologi Kejuruteraan Mekanikal dan Pembuatan, University Teknikal Malaysia Melaka, Hang Tuah Jaya, 76100 Durian Tunggal, Melaka, Malaysia*
[3] *Forecasting and Engineering Technology Analysis (FETA) Research Group, University Teknikal Malaysia Melaka, Hang Tuah Jaya, 76100 Durian Tunggal, Melaka, Malaysia*

(Received 26 September 2023; Accepted 7 November 2023)

In this paper, the derivation of hyper-singular integral equations (HSIEs) for thermoelectric bonded materials (TEBM) featuring a crack parallel to interface subject to in-plane shear stress τ_{xy}^{∞} was intensively studied. Generally, stress intensity factors (SIFs) were calculated using HSIEs with the help of modified complex stress variable function (MCSVF), and continuity conditions of the resultant electric force and displacement electric function. The unknown crack opening displacement (COD) function, electric current density, and energy flux load are mapped into the square root singularity function using the curved length coordinate method as the right-hand term. This unknown function is then used to compute the dimensionless SIFs in order to determine the stability behavior of TEBM featuring a crack parallel to interface subject to in-plane shear stress τ_{xy}^{∞}. Numerical results of the dimensionless SIFs at all the crack tips are presented. Our results are totally in good agreement with those of the previous works. It is observed that the dimensionless SIFs at the crack tips depend on the elastic constants ratio, the crack geometries, the electric conductivity, and the thermal expansion coefficients.

Keywords: *thermoelectric; bonded materials; single crack; hyper-singular integral equations; stress intensity factors.*

2010 MSC: 74A45, 74G70, 74S70 **DOI:** 10.23939/mmc2023.04.1230

1. Introduction

Thermoelectric bonded materials (TEBM) featuring a crack have become an intriguing area of research due to their potential implications on the performance and reliability of thermoelectric devices. TEBM, which can convert heat into electrical energy and vice versa, has gained considerable attention as an eco-friendly and energy-efficient solution for waste heat recovery and power generation. However, the presence of cracks in these materials can significantly influence their mechanical and thermoelectric behavior, leading to reduced efficiency and increased susceptibility to failure. A considerable number of researchers have been motivated to explore the mechanical and thermoelectric behavior of TEBM, with a specific focus on challenges such as interface cracks, curve cracks, or slanted cracks.

Examining an interface crack subjected to a remote electric current within TEBM, Song et al. [1] employed complex stress variable functions (CSVF) to analyze the thermal stress intensity factors (SIFs) at the crack tips. Their findings demonstrated that the presence of the electric current could lead to varying effects on the thermal SIFs. Depending on the specific parameters characterizing the

This work was supported by the Ministry of Higher Education Malaysia through the Fundamental Research Grant Scheme (FRGS/1/2021/STG06/UTEM/03/2). The authors also gladly appreciate the support from University Teknikal Malaysia Melaka.

bonded materials, the electric current could either amplify or diminish the thermal SIFs. As highlighted by Jiang and Zhou [2], the SIFs in the context of dual collinear interface cracks within TEBM, under combined electric and thermal loads, experience alterations due to several factors: crack length, crack spacing, and the ratio of bi-elastic constants. These researchers approached the problem by employing Laplace equations and considering the driving influences originating from electric current density and energy flux. These driving forces have implications for the electric potential and temperature distributions within the material. Using the CSVF method, Cui et al. [3] investigated the fatigue crack propagation behavior in a temperature-dependent TEBM connected to an elastic substrate under cyclic thermal loading. Their findings underscore that the interface between the thermoelectric layer and the substrate is the preferential location for crack propagation. Examining the scenario of an interfacial crack within imperfectly bonded TEBM containing an elliptical inclusion, Du et al. [4] employed conformal mapping and complex function methods. The material was subjected to uniform heat flux and energy flux conditions extending to infinity. Their findings revealed that the inclusion's presence led to a decrease in the conversion efficiency of the TEBM. Jiang and Zhou [5] conducted an investigation into how dual collinear interface cracks affect the electric potential and temperature distribution in a TEBM system. This system was subjected to both electric and thermal loads. To analyze this, they employed Laplace equations alongside the driving forces arising from electric current density and energy flux. Through numerical simulations, they revealed the significant influence of parameters such as crack length, crack spacing, and layer thickness ratio on the SIFs of electric current density and energy flux around the crack tip. These effects remained pronounced under the conditions of constant electric and thermal loads. In their study, Nourazar et al. [6] utilized the Fourier transform method with an unknown density to address the mixed-mode problem involving a curved crack within a piezoelectric bonded materials. The crack was subjected to a general in-plane thermal load. Their analysis revealed that the dimensionless SIFs were significantly influenced by factors such as the crack's length, radius, and the distance from the temperature disturbance.

Hyper-singular integral equations (HSIEs) have found extensive application in various physics and engineering fields, notably in tackling crack-related challenges within fracture mechanics [7–10]. This method stands out due to its numerous advantages over other commonly employed crack analysis techniques. It offers enhanced efficiency, a more accurate depiction of crack tip behavior, adaptability for different crack configurations, and the direct extraction of crack opening displacement (COD) function from the equation's solution. However, alongside these benefits, HSIEs come with certain limitations. Their formulation and solution can be more intricate compared to simpler approaches like the boundary element method. Moreover, addressing crack tip singularities and ensuring precise integration techniques are required to obtain accurate solutions. Despite these considerations, HSIEs remain an invaluable tool in crack analysis, significantly advancing the understanding and prediction of crack behavior across various engineering applications. To the authors' best knowledge, there is limited available information concerning the application of HSIEs to formulate crack-related problems within TEBM exposed to remote stress. To address this gap, the present study introduces a novel approach by employing the modified CSVF (MCSVF) method to transform the problem into HSIEs. This transformation is facilitated by adhering to continuity conditions governing the resultant electric force and electric displacement function, as well as temperature and resultant heat flux, across the TEBM. Consequently, this study offers a pioneering investigation into the dimensionless SIFs at the tip of a crack parallel to an interface situated in the upper part of the TEBM, all while being subjected to in-plane shear stress $\tau_{xy}^{\infty} = \tau$.

2. Mathematical formulation

Consider a crack parallel to interface lie in the upper part of TEBM subject to in-plane shear stress $\tau_{xy}^{\infty} = \tau$ as shown in Figure 1. Note that, G_i is shear modulus, κ_i is thermal conductivity, λ_i is electric conductivity, $\boldsymbol{J}$ is electric current density vector for $i = 1$ and $i = 2$ represent upper and lower parts of

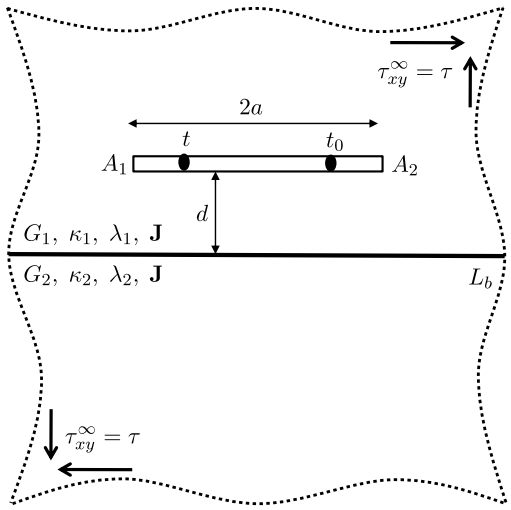

Fig. 1. A crack parallel to interface lie in the upper part of TEBM subject to in-plane shear stress τ_{xy}^{∞}.

TEBM, respectively, L_b is bonded materials interface and $2a$ is the length of the crack. According to Todoroki [11], the equation governing electric current is given by

$$\boldsymbol{J} = -\lambda \nabla \vartheta(z), \tag{1}$$

$$\vartheta = f(z) + \overline{f(z)} + N_1, \tag{2}$$

where ϑ is electric CSVF represent by $f(z)$ and its conjugate, N_1 is real constant and $z = x+iy$. The conditions for strain components ε for upper (subscript 1) and lower ((subscript 2) parts of TEBM is

$$\varepsilon_{x_1y_1} = \varepsilon_{x_2y_2}. \tag{3}$$

Those strains can be defined by Young's modulus of elasticity E and stress components τ as

$$\varepsilon_{x_1y_1} = \frac{1+v_1}{E_1}\tau_{x_1y_1}^{\infty},\ \varepsilon_{x_2y_2} = \frac{1+v_2}{E_2}\tau_{x_2y_2}^{\infty}, \tag{4}$$

where $E_i = 2G_i(1+v_i)$ and $i = 1, 2$. For in-plane stress, we have $\tau_{x_1y_1} = \tau_{x_2y_2} = \tau$ and applying condition in Eq. (3), then Eq. (4) is reduced to

$$\frac{1+v_1}{E_1}\tau_{x_1y_1}^{\infty} = \frac{1+v_2}{E_2}\tau_{x_2y_2}^{\infty}. \tag{5}$$

In accordance with the study by Song et al. [1], the stress components $(\sigma_x, \sigma_y, \sigma_{xy})$, resultant electric force (X, Y), and displacement electric functions (u, v) resulting from the thermoelectric function can be ascertained using the subsequent expressions

$$\sigma_x + \sigma_y = 2[\phi'(z) + \overline{\psi'(z)}] + \frac{E\alpha\lambda}{\kappa} f(z)\overline{f(z)} \tag{6}$$

$$\sigma_y - \sigma_x + 2i\sigma_{xy} = 2[\bar{z}\phi''(z) + \psi'(z)] + \frac{E\alpha\lambda}{\kappa} f'(z)\overline{F(z)} \tag{7}$$

$$-Y + iX = \phi(z) + z\overline{\phi'(z)} + \overline{\psi(z)} + \frac{E\alpha\lambda}{4G\kappa} F(z)\overline{f(z)} \tag{8}$$

$$u + iv = \frac{1}{2G}\big[K\phi(z) - z\overline{\phi'(z)} - \overline{\psi(z)}\big] + \alpha \int \Omega(z)\, dz - \frac{E\alpha\lambda}{4G\kappa} F(z)\overline{f(z)}, \tag{9}$$

where $K = (3-\mu)/(1+\mu)$, μ is Poisson's ratio, α is the coefficient of thermal expansion, $\Omega(z) = -(\lambda/\kappa)f(z)^2 + (2/\kappa)g(z)$, $F(z) = \int f(z)\, dz$, and $\phi(z)$, $\psi(z)$, and $g(z)$ are CSVF. The derivative of Eq. (8) with respect to z yields the normal (N) and tangential (T) components as follows

$$\frac{d}{dz}\{-Y+iX\} = \phi'(z) + \overline{\phi'(z)} + \frac{d\bar{z}}{dz}\big(z\overline{\phi''(z)} + \overline{\psi'(z)}\big) + \frac{E\alpha\lambda}{4G\kappa}\left(f(z)\overline{f(z)} + F(z)\overline{f'(z)}\frac{d\bar{z}}{dz}\right) = N + iT, \tag{10}$$

where $d\bar{z}/dz = -e^{-2i\theta}$ and θ is the tangential angle along the segment $\overline{z, z+dz}$.

In the context of research by Nik Long and Eshkuvatov [12] as well as Song et al. [1], the CSVF and the non-established analytic functions governing the electric and thermal fields in the context of a crack within an infinite material can be represented as follows

$$\phi(z) = \frac{1}{2\pi}\int_L \frac{g(t)dt}{t-z}, \tag{11}$$

$$\psi(z) = \frac{1}{2\pi}\int_L \frac{\overline{g(t)}\, dt}{t-z} + \frac{1}{2\pi}\int_L g(t)\left(\frac{d\bar{t}}{t-z} - \frac{\bar{t}\, dt}{(t-z)^2}\right), \tag{12}$$

$$f(z) = \frac{i\,\boldsymbol{J}}{2\lambda}\sqrt{z^2-a^2}, \tag{13}$$

$$F(z) = \frac{i\,\boldsymbol{J}}{4\lambda}\big(z\sqrt{z^2-a^2} - a^2\ln\big(z+\sqrt{z^2-a^2}\big)\big), \tag{14}$$

$$g(z) = \frac{i\boldsymbol{U}}{2}\sqrt{z^2 - a^2}, \tag{15}$$

$$\Omega(z) = \frac{\boldsymbol{J}^2}{4\lambda\kappa}(z^2 - a^2) + \frac{i\boldsymbol{U}}{\kappa}\sqrt{z^2 - a^2}, \tag{16}$$

where $g(t)$ is the COD function defined as

$$g(t) = \frac{2G}{i(K+1)}\left[(u(t) + iv(t))^+ - (u(t) + iv(t))^-\right], \quad (t \in L), \tag{17}$$

$(u(t) + iv(t))^+$ and $(u(t) + iv(t))^-$ denote the displacements at a point t of the upper and lower crack faces, respectively.

According to Chen and Hasebe [13], and proven by Hamzah et al. [14], the MCSVF for the crack lies in the upper part of TEBM are defined as

$$\phi_1(z) = \phi_{1p}(z) + \phi_{1c}(z), \quad \psi_1(z) = \psi_{1p}(z) + \psi_{1c}(z), \tag{18}$$

where $\phi_{1p}(z)$ and $\psi_{1p}(z)$ are the principal part of the CSVF and the elementary solution for isotropic medium (infinite materials), whereas $\phi_{1c}(z)$ and $\psi_{1c}(z)$ are the complement part of the CSVF. The CSVFs for the crack lies in the lower part of TEBM represented by $\phi_2(z)$ and $\psi_2(z)$. The continuity condition of Eqs. (8) and (9), and applying (18) give

$$\left[\phi_{1p}(t) + \phi_{1c}(t) + t\,\overline{\phi'_{1p}(t)} + \overline{\psi_{1p}(t)} + t\,\overline{\phi'_{1c}(t)} + \overline{\psi_{1c}(t)} + \frac{E_1\alpha_1\lambda_1}{4G_1\kappa_1}\left(F_{1p}(t)\overline{f_{1p}(t)} + F_{1c}(t)\overline{f_{1c}(t)}\right)\right]^+$$
$$= \left[\phi_2(t) + t\,\overline{\phi'_2(t)} + \overline{\psi_2(t)} + \frac{E_2\alpha_2\lambda_2}{4G_2\kappa_2}F_2(t)\overline{f_2(t)}\right]^-, \tag{19}$$

$$G_2\Bigg[K_1\phi_{1p}(t) + K_1\phi_{1c}(t) - \left(t\,\overline{\phi'_{1p}(t)} + \overline{\psi_{1p}(t)}\right) - \left(t\,\overline{\phi'_{1c}(t)} + \overline{\psi_{1c}(t)}\right)$$
$$+ 2G_1\alpha_1\left(\int \Omega_{1p}(t)\,dt + \int \Omega_{1c}(t)\,dt\right) - \frac{E_1\alpha_1\lambda_1}{2\kappa_1}\left(F_{1p}(t)\,\overline{f_{1p}(t)} + F_{1c}(t)\,\overline{f_{1c}(t)}\right)\Bigg]^+$$
$$= G_1\left[K_2\phi_2(t) - t\,\overline{\phi'_2(t)} - \overline{\psi_2(t)} + 2G_2\alpha_2\int \Omega_2(t)\,dt - \frac{E_2\alpha_2\lambda_2}{2\kappa_2}F_2(t)\,\overline{f_2(t)}\right]^-. \tag{20}$$

Since the temperature and resultant heat flux are continuous across the crack bonded materials interface and apply MCSVF yields

$$\left[f_{1p}(t) + f_{1c}(t) + \overline{f_{1p}(t)} + \overline{f_{1c}(t)}\right]^+ = \left[f_2(t) + \overline{f_2(t)}\right]^-, \tag{21}$$

$$\lambda_1\left[f_{1p}(t) + f_{1c}(t) - \overline{f_{1p}(t)} - \overline{f_{1c}(t)}\right]^+ = \lambda_2\left[f_2(t) - \overline{f_2(t)}\right]^-. \tag{22}$$

By applying analytical continuation to Eqs. (21) and (22), the following expressions are obtainable

$$f_{1c}(z) = \frac{\lambda_1 - \lambda_2}{\lambda_1 + \lambda_2}\,\overline{f_{1p}}(z), \quad z \in S_1 + L_b, \tag{23}$$

$$f_2(z) = \frac{2\lambda_1}{\lambda_1 + \lambda_2}f_{1p}(z), \quad z \in S_2 + L_b. \tag{24}$$

Similar to thermal CSVF yields

$$g_{1c}(z) = \frac{\kappa_1 - \kappa_2}{\kappa_1 + \kappa_2}\overline{g_{1p}}(z), \quad z \in S_1 + L_b, \tag{25}$$

$$g_2(z) = \frac{2\kappa_1}{\kappa_1 + \kappa_2}g_{1p}(z), \quad z \in S_2 + L_b. \tag{26}$$

By applying analytical continuation to Eqs. (19) and (20), and substituted with Eqs. (23), (24), (25) and (26) the following expressions are obtainable

$$\phi_{1c}(z) = \Gamma_1\left(z\,\overline{\phi'_{1p}}(z) + \overline{\psi_{1p}}(z)\right) + \Gamma_2\overline{F_{1p}}(z)f_{1p}(z) + \Gamma_3\int \overline{f_{1p}}^2(z)\,dz - \Gamma_4\int \overline{g_{1p}}(z)\,dz, \tag{27}$$

$$\psi_{1c}(z) = \Gamma_5\overline{\phi_{1p}}(z) - z\phi'_{1c}(z) + \Gamma_6\overline{F_{1p}}(z)f_{1p}(z) + \Gamma_7\int \overline{\Omega_{1p}}(z)\,dz + \Gamma_8\int \overline{f_{1p}}^2(z)\,dz - \Gamma_9\int \overline{g_{1p}}(z)\,dz, \tag{28}$$

$$\phi_2(z) = \Gamma_{10}\phi_{1p}(z) + \Gamma_{11}F_{1p}(z)\overline{f_{1p}}(z) + \Gamma_{12}F_{1p}(z)\overline{f_{1p}}(z) + \Gamma_7\int \Omega_{1p}(z)\,dz + \Gamma_8\int f_{1p}^2(z)\,dz - \Gamma_9\int g_{1p}(z)\,dz, \tag{29}$$

$$\psi_2(z) = \Gamma_{13}\big(z\,\phi_{1p}'(z) + \psi_{1p}(z)\big) - z\,\phi_2'(z) + \Gamma_{14}F_{1p}(z)\overline{f_{1p}}(z) + \Gamma_{15}\int f_{1p}^2(z)\,dz - \Gamma_{16}\int g_{1p}(z)\,dz, \tag{30}$$

where $\overline{\phi_{1p}}(z) = \overline{\phi_{1p}(\bar{z})}$, and Γ_j are bi-elastic constants ratio defined as

$$\Gamma_1 = \frac{G_2 - G_1}{G_1 + G_2K_1}, \quad \Gamma_2 = \frac{(2G_2-1)E_1\alpha_1\lambda_1}{4\kappa_1(G_1+G_2K_1)}\left(\frac{\lambda_1-\lambda_2}{\lambda_1+\lambda_2}\right)^2, \quad \Gamma_3 = \frac{2G_1G_2\alpha_1\lambda_1}{\kappa_1(G_1+G_2\kappa_1)}\left(\frac{\lambda_1-\lambda_2}{\lambda_1+\lambda_2}\right)^2,$$
$$\Gamma_4 = \frac{4G_1G_2\alpha_1}{\kappa_1(G_1+G_2\kappa_1)}\left(\frac{\kappa_1-\kappa_2}{\kappa_1+\kappa_2}\right), \quad \Gamma_5 = \frac{G_2K_1 - G_1K_2}{G_1K_2+G_2},$$
$$\Gamma_6 = \left(\frac{E_2\alpha_2\lambda_2(2G_1G_2+G_1K_2)}{4G_2\kappa_2(G_1K_2+G_2)}\right)\left(\frac{2\lambda_1}{\lambda_1+\lambda_2}\right)^2, \quad \Gamma_7 = \frac{2G_1G_2\alpha_1}{(G_1K_2+G_2)},$$
$$\Gamma_8 = \frac{2G_1G_2\alpha_2\lambda_2}{\kappa_2(G_1K_2+G_2)}\left(\frac{2\lambda_1}{\lambda_1+\lambda_2}\right)^2, \quad \Gamma_9 = \frac{8G_1G_2\alpha_2\kappa_1}{\kappa_2(\kappa_1+\kappa_2)(G_1K_2+G_2)}, \quad \Gamma_{10} = \frac{(K_1+1)G_2}{G_1K_2+G_2},$$
$$\Gamma_{11} = \frac{E_2\alpha_2\lambda_2(2G_1-1)}{4\kappa_2(G_1K_2+G_2)}\left(\frac{2\lambda_1}{\lambda_1+\lambda_2}\right)^2, \quad \Gamma_{12} = \frac{G_2E_1\alpha_1\lambda_1(1-2G_1)}{4G_1\kappa_1(G_1K_2+G_2)}, \Gamma_{13} = \frac{G_2(1+K_1)}{G_1+G_2K_1},$$
$$\Gamma_{14} = \frac{(K_1+2G_1)G_2E_1\alpha_1\lambda_1}{4G_1\kappa_1(G_1+G_2K_1)}\left(\frac{\lambda_1-\lambda_2}{\lambda_1+\lambda_2}\right)^2, \quad \Gamma_{15} = \frac{2G_1G_2\alpha_1\lambda_1}{\kappa_1(G_1+G_2K_1)}\left(\frac{\lambda_1-\lambda_2}{\lambda_1+\lambda_2}\right)^2,$$
$$\Gamma_{16} = \frac{4G_1G_2\alpha_1}{\kappa_1(G_1+G_2K_1)}\left(\frac{\kappa_1-\kappa_2}{\kappa_1+\kappa_2}\right)$$

In order to formulate the HSIEs for a crack parallel to interface lie in the upper part of TEBM, we need to define two traction components which are $[N(t_0)+iT(t_0)]_{1p}$ and $[N(t_0)+iT(t_0)]_{1c}$ for the principle and complementary parts, respectively. These traction components are obtained when the observation point is placed at the point, t_0 ($t_0 \in L$), caused by COD function $g(t)$ at $t \in L$, substituting Eqs. (27) and (28) into Eq. (10), and applying Eqs. (11)–(16) which gives

$$\big[N(t_0)+iT(t_0)\big]_1 = \frac{1}{\pi}\oint_L \frac{g(t)\,dt}{(t-t_0)^2} + \frac{1}{2\pi}\int_L M_1(t,t_0)g(t)\,dt + \frac{1}{2\pi}\int_L M_2(t,t_0)\overline{g(t)}dt + M_3(a,t_0), \tag{31}$$

where

$$M_1(t,t_0) = -\frac{1}{(t-t_0)^2} + \frac{1}{(\bar{t}-\bar{t}_0)^2}\frac{d\bar{t}}{dt}\frac{d\bar{t}_0}{dt_0} + \Gamma_1\left[\frac{1}{(t-\bar{t}_0)^2} + \frac{2(\bar{t}_0-\bar{t})}{(t-\bar{t}_0)^3} + \left(\frac{1}{(\bar{t}-t_0)^2} + \frac{1}{(t-\bar{t}_0)^2}\right)\frac{d\bar{t}}{dt}\right.$$
$$\left. + \left(\frac{2(2t_0-3\bar{t}_0+\bar{t})}{(t-\bar{t}_0)^3} - \frac{6(\bar{t}_0-\bar{t})(\bar{t}_0-t_0)}{(t-\bar{t}_0)^4} - \left(\frac{1}{(t-\bar{t}_0)^2} + \frac{2(\bar{t}_0-t_0)}{(t-\bar{t}_0)^3}\right)\frac{d\bar{t}}{dt} - \frac{1}{(t-\bar{t}_0)^2}\right)\frac{d\bar{t}_0}{dt_0}\right]$$
$$+ \Gamma_5\frac{1}{(t-\bar{t}_0)^2}\frac{d\bar{t}_0}{dt_0};$$
$$M_2(t,t_0) = \frac{1}{(\bar{t}-\bar{t}_0)^2}\frac{d\bar{t}}{dt} + \left(\frac{1}{(\bar{t}-\bar{t}_0)^2} + \frac{2(t_0-t)}{(\bar{t}-\bar{t}_0)^3}\frac{d\bar{t}}{dt}\right)\frac{d\bar{t}_0}{dt_0} + \Gamma_1\left[\frac{1}{(\bar{t}-t_0)^2} + \frac{1}{(t-\bar{t}_0)^2}\right.$$
$$\left. + \left(\frac{1}{(\bar{t}-t_0)^2} + \frac{2(t_0-t)}{(\bar{t}-\bar{t}_0)^3}\right)\frac{d\bar{t}}{dt} + \left(\frac{2(t_0-\bar{t}_0)}{(t-\bar{t}_0)^3} - \frac{1}{(t-\bar{t}_0)^2}\right)\frac{d\bar{t}_0}{dt_0}\right];$$
$$M_3(a,t_0) = \Gamma_2\frac{\boldsymbol{J}^2}{4\lambda_1^2}\left(t_0^2 - a^2 + \frac{t_0}{2\sqrt{t_0^2-a^2}}\left(t_0\sqrt{t_0^2-a^2} - a^2\ln\left(t_0+\sqrt{t_0^2-a^2}\right)\right)\right)$$
$$+ \left(\Gamma_2 + (\Gamma_6-\Gamma_2)\frac{d\bar{t}_0}{dt_0}\right)\frac{\boldsymbol{J}^2}{4\lambda_1^2}\left(\bar{t}_0^2 - a^2 + \frac{\bar{t}_0}{2\sqrt{\bar{t}_0^2-a^2}}\left(\bar{t}_0\sqrt{\bar{t}_0^2-a^2} - a^2\ln\left(\bar{t}_0+\sqrt{\bar{t}_0^2-a^2}\right)\right)\right)$$
$$+ \Gamma_2\frac{\boldsymbol{J}^2}{4\lambda_1^2}(t_0-\bar{t}_0)\left(3\bar{t}_0 + \left(\bar{t}_0\sqrt{\bar{t}_0^2-a^2} - a^2\ln\left(\bar{t}_0+\sqrt{\bar{t}_0^2-a^2}\right)\right)\frac{(\bar{t}_0^2-\bar{t}_0-a^2)}{2\left(\sqrt{\bar{t}_0^2-a^2}\right)^3}\right)\frac{d\bar{t}_0}{dt_0}$$

$$
\begin{aligned}
&+\Gamma_3\frac{\boldsymbol{J}^2}{4\lambda_1^2}\left(2a^2-t_0^2-\bar{t}_0^2+(3\bar{t}_0^2-2t_0\bar{t}_0-a^2)\frac{d\bar{t}_0}{dt_0}\right)\\
&+\Gamma_4\frac{i\boldsymbol{U}}{2}\left(\sqrt{t_0^2-a^2}-\sqrt{\bar{t}_0^2-a^2}+\frac{2\bar{t}_0^2-\bar{t}_0t_0-a^2}{\sqrt{\bar{t}_0^2-a^2}}\frac{d\bar{t}_0}{dt_0}\right)\\
&+\left[\left(\frac{\Gamma_7}{\kappa_1}-\frac{\Gamma_8}{\lambda_1}\right)\frac{\boldsymbol{J}^2}{4\lambda_1}(\bar{t}_0^2-a^2)+\left(\frac{\Gamma_7}{\kappa_1}-\frac{\Gamma_9}{2}\right)i\boldsymbol{U}\sqrt{\bar{t}_0^2-a^2}\right]\frac{d\bar{t}_0}{dt_0}\\
&+(\Gamma_{17}+\Gamma_{18})\frac{\boldsymbol{J}^2}{4\lambda_1^2}\left[\sqrt{t_0^2-a^2}\sqrt{\bar{t}_0^2-a^2}\right.\\
&\quad\left.+\left(t_0\sqrt{t_0^2-a^2}-a^2\ln\left(t_0+\sqrt{t_0^2-a^2}\right)\right)\frac{\bar{t}_0}{2\sqrt{\bar{t}_0^2-a^2}}\frac{d\bar{t}_0}{dt_0}\right]
\end{aligned}
$$

and

$$\Gamma_{17}=\frac{E_1\alpha_1\lambda_1}{4G_1\kappa_1},\quad \Gamma_{18}=\frac{E_1\alpha_1\lambda_1}{4G_1\kappa_1}\left(\frac{\kappa_1-\kappa_2}{\kappa_1+\kappa_2}\right)^2.$$

Note that the first integral with the equal sign in Eq. (31) represents the hypersingular integral and must be defined as a finite part integral. In order to solve this HSIEs, the curved length coordinate method and quadrature formulas introduced by [15–18] is used.

3. Numerical results and discussion

In order to investigate the behavior of non-dimensional SIFs for crack problems in thermoelectric bonded materials subjected to remote stress, we define the SIFs at the crack tip A_j as follows

$$K_{A_j}=(K_1-iK_2)_{A_j}=\sqrt{2\pi}\lim_{t\to t_{A_j}}\sqrt{|t-t_{A_j}|}\,g_1'(t_1),\quad j=1,2, \tag{32}$$

where $g_1'(t_1)$ is defined as follows

$$g_1'(t_1)|_{t_1=t_1(s_1)}=\frac{-s_1H_1(s_1)}{\sqrt{a_1^2-s_1^2}}e^{-i\theta_{A_j}},\quad H_1'(s_1)=0. \tag{33}$$

Table 1. Dimensionless SIFs for a crack parallel to the interface of TEBM as illustrated in Figure 1

SIFs	M	$d/2a$								
		0.1	0.2	0.3	0.4	0.5	0.6	0.7	0.8	0.9
F_{1A_1}	10	0.0864	0.0661	0.0519	0.0402	0.0309	0.0238	0.0186	0.0149	0.0123
	15	0.0886	0.0663	0.0521	0.0405	0.0313	0.0243	0.0193	0.0157	0.0132
	20	0.0888	0.0665	0.0524	0.0409	0.0317	0.0248	0.0199	0.0165	0.0142
	25	0.0888	0.0665	0.0524	0.0409	0.0317	0.0248	0.0199	0.0165	0.0142
F_{2A_1}	10	1.0977	1.0515	1.0376	1.0307	1.0262	1.0226	1.0196	1.0171	1.0150
	15	1.0872	1.0516	1.0377	1.0309	1.0264	1.0229	1.0200	1.0175	1.0155
	20	1.0867	1.0517	1.0379	1.0311	1.0266	1.0232	1.0203	1.0179	1.0159
	25	1.0867	1.0517	1.0379	1.0311	1.0266	1.0232	1.0203	1.0179	1.0159
F_{1A_2}	10	-0.0856	-0.0653	-0.0509	-0.0389	-0.0293	-0.0218	-0.0161	-0.0118	-0.0085
	15	-0.0876	-0.0651	-0.0506	-0.0386	-0.0289	-0.0213	-0.0154	-0.011	-0.0076
	20	-0.0874	-0.0649	-0.0504	-0.0383	-0.0285	-0.0208	-0.0148	-0.0102	-0.0066
	25	-0.0874	-0.0649	-0.0504	-0.0383	-0.0285	-0.0208	-0.0148	-0.0102	-0.0066
F_{2A_2}	10	1.0976	1.0512	1.0370	1.0300	1.0252	1.0215	1.0183	1.0156	1.0133
	15	1.0870	1.0511	1.0369	1.0298	1.0250	1.0212	1.0180	1.0152	1.0129
	20	1.0864	1.0510	1.0368	1.0296	1.0248	1.0209	1.0177	1.0149	1.0125
	25	1.0864	1.0510	1.0368	1.0296	1.0248	1.0209	1.0177	1.0149	1.0125

Table 1 displays convergence test results on the Mode I (F_1) and Mode II (F_2) dimensionless SIFs at the crack tips A_1 and A_2 for a crack parallel to the interface lie in the upper part of TEBM subject to in-plane shear stress τ_{xy}^{∞} for $G_2/G_1=0.5$, $\boldsymbol{J}=10$, $\boldsymbol{U}=0$, and $d/2a$ varies as illustrated in Figure 1. The level of accuracy in the numerical outcomes relies on how finely we subdivide the cracks, denoted by the parameter M. To gauge the convergence of the results, we incrementally increase the value

of M, commencing from $M = 10$ and progressing sequentially through $M = 15$ and $M = 20$. Our progression concludes at $M = 25$ when the dimensionless values of SIFs align with those obtained from the previous M values, as elaborated in Table 1. Notably, it is evident that employing smaller M values generates convergent numerical results.

Table 2. Dimensionless SIFs for a crack parallel to the interface of TEBM compared with Isida and Noguchi [19].

SIFs	$d/2a$								
	0.1	0.2	0.3	0.4	0.5	0.6	0.7	0.8	0.9
F_{1A_1}*	0.0881	0.0657	0.0514	0.0396	0.0301	0.0228	0.0174	0.0133	0.0104
F_{1A_1}**	0.0880	0.0660	0.0520	0.0400	0.0300	0.0230	0.0170	0.0130	0.0100
F_{2A_1}*	1.0865	1.0514	1.0373	1.0303	1.0257	1.0220	1.0190	1.0164	1.0142
F_{2A_1}**	1.0860	1.0510	1.0370	1.0300	1.0260	1.0220	1.0190	1.0160	1.0140
F_{1A_2}*	-0.0881	-0.0657	-0.0514	-0.0396	-0.0301	-0.0228	-0.0174	-0.0133	-0.0104
F_{2A_2}*	1.0865	1.0514	1.0373	1.0303	1.0257	1.0220	1.0190	1.0164	1.0142

*Current study, **Isida and Noguchi [19].

On the other hand, Table 2 provides a display of the dimensionless SIFs in cases where $G_2/G_1 = 0.5$, $\boldsymbol{J} = \boldsymbol{U} = 0$, $M = 25$, and the parameter $d/2a$ is subject to variation. Our computational findings exhibit complete concurrence with the results documented by Isida and Noguchi [19]. An interesting observation is that the F_1 value at crack tip A_1 mirrors the negative value of F_1 at crack tip A_2. Conversely, the F_2 value at crack tip A_1 perfectly matches the F_2 value at crack tip A_2. This phenomenon is attributed to the equivalence in stress distribution at the respective crack tips.

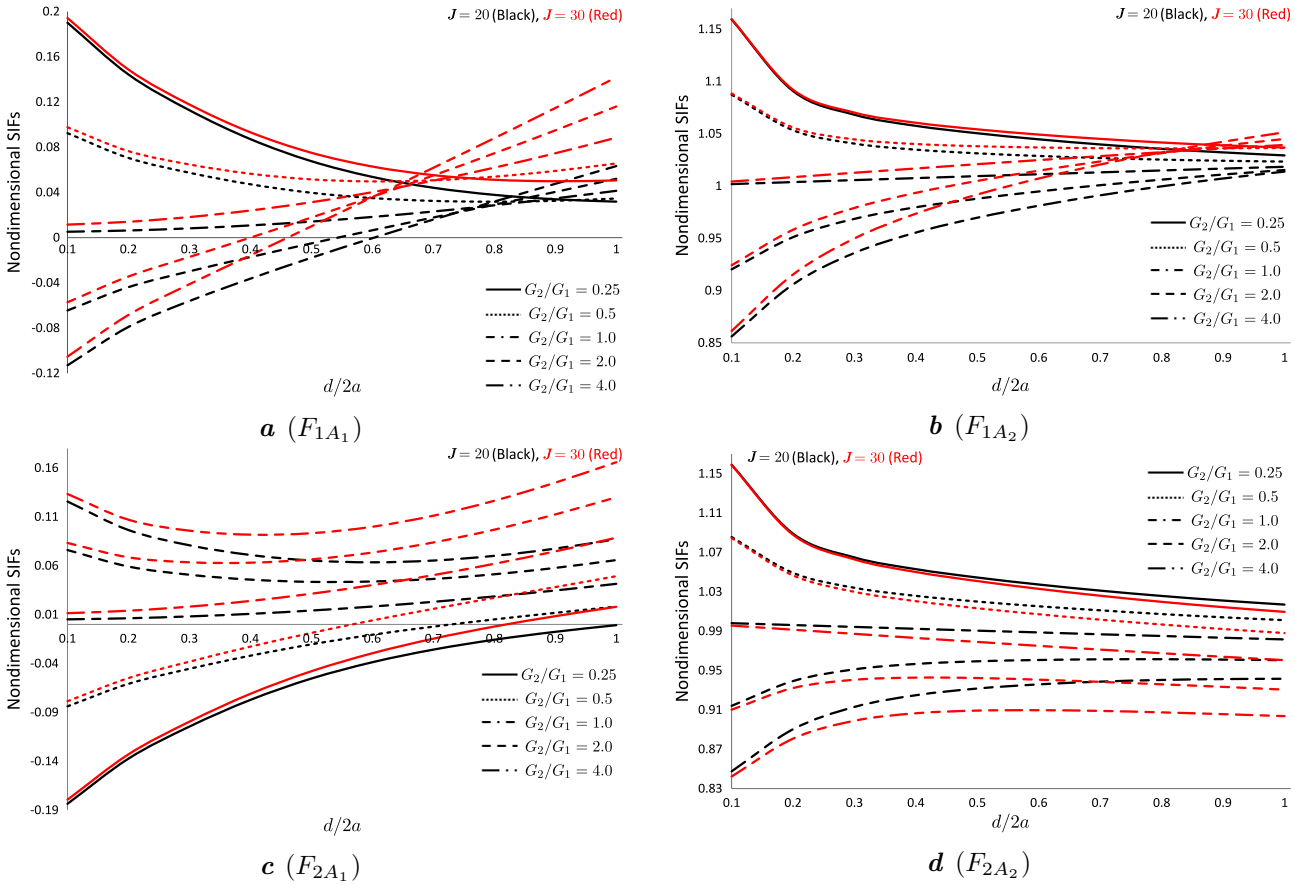

Fig. 2. Dimensionless SIFs at the crack tips A_1 and A_2 for $\boldsymbol{J} = 20$ (black) and $\boldsymbol{J} = 30$ (red).

Figure 2 displays the F_1 and F_2 dimensionless SIFs at the crack tips A_1 and A_2 for a crack parallel to the interface lie in the upper part of TEBM subject to in-plane shear stress τ_{xy}^{∞} for $\boldsymbol{J} = 20$ (black), $\boldsymbol{J} = 30$ (red), $\boldsymbol{U} = 0$, and $d/2a$ varies. It is found that F_1 for $\boldsymbol{J} = 30$ (red) at crack tips A_1 and A_2

is higher than F_1 for $\boldsymbol{J} = 20$ (black). As G_2/G_1 increases F_1 decreases at all cracks tips. However F_2 increases at tip A_1 and decreases at tip A_2. Whereas as $d/2a$ increases F_1 decreases at crack tips A_1 and A_2 for $G_2/G_1 < 1.0$, and increases for $G_2/G_1 \geqslant 1.0$. These numerical results provide evidence that as $\boldsymbol{J}$ increases, the materials exhibit a decrease in strength, whereas an increase in G_2/G_1 leads to greater stability.

4. Conclusions

In this study, we have addressed the presence of a crack parallel to an interface located in the upper part of TEBM and subjected to in-plane shear stress τ_{xy}^{∞}. Although the problem itself has a long history, our research introduces several novel elements. Notably, the MCSVF technique utilized in this work is a traditional approach for solving crack-related challenges in bonded materials. However, its application to crack problems within the realm of TEBM represents a fresh perspective. Our approach leads to the formulation of HSIEs, wherein the core unknowns involve the COD function, electric current density, and energy flux load between the crack tips. Through our examination of benchmark problems, our numerical results showcase accelerated convergence, and our analyses align closely with outcomes from previous investigations. Building upon this study, we envision numerous avenues for extension. These possibilities encompass the incorporation of cohesive models, exploration of cracks at interfaces of bonded materials, analysis of cracks originating from inclusions, and the investigation of three-dimensional crack problems within the context of TEBM. Ongoing research endeavors are actively expanding the scope of application for this newly developed conceptual framework.

[1] Song K., Song H. P., Schiavone P., Gao C. F. Electric current induced thermal stress around a bi-material interface crack. Engineering Fracture Mechanics. **208**, 1–12 (2019).

[2] Jiang D., Zhou Y.-T. Role of crack length, crack spacing and layer thickness ratio in the electric potential and temperature of thermoelectric bi-materials systems. Engineering Fracture Mechanics. **259**, 108170 (2022).

[3] Cui Y. J., Wang K. F., Zheng L., Wang B. L., Zhang C. W. Theoretical model of fatigue crack growth of a thermoelectric pn-junction bonded to an elastic substrate. Mechanics of Materials. **151**, 103623 (2020).

[4] Du X.-K., Zhang Y.-L., Ding S.-H. Exact solutions of interfacial cracking problem of elliptic inclusion in thermoelectric material. In E3S Web of Conferences. **261**, 02089 (2021).

[5] Jiang D., Zhou Y.-T. Role of crack length, crack spacing and layer thickness ratio in the electric potential and temperature of thermoelectric bi-materials systems. Engineering Fracture Mechanics. **259**, 108170 (2022).

[6] Nourazar M., Yang W., Chen Z. Fracture analysis of a curved crack in a piezoelectric plane under general thermal loading. Engineering Fracture Mechanics. **284**, 109208 (2023).

[7] Dutta B., Banerjea S. Solution of a hypersingular integral equation in two disjoint intervals. Applied Mathematics Letters. **22** (8), 1281–1285 (2009).

[8] Hamzah K. B., Nik Long N. M. A., Senu N., Eshkuvatov Z. K. Stress intensity factor for bonded dissimilar materials weakened by multiple cracks. Applied Mathematical Modelling. **77** (1), 585–601 (2020).

[9] Hamzah K. B., Nik Long N. M. A., Senu N., Eshkuvatov Z. K. Numerical solution for crack phenomenon in dissimilar materials under various mechanical loadings. Symmetry. **13** (2), 235 (2021).

[10] Elahi M. R., Mahmoudi Y., Salimi Shamloo A., Jahangiri Rad M. A novel collocation method for numerical solution of hypersingular integral equation with singular right-hand function. Advances in Mathematical Physics. **2023**, 5845263 (2023).

[11] Todoroki A. Electric current analysis of CFRP using perfect fluid potential flow. Transactions of the Japan Society for Aeronautical and Space Sciences. **55** (3), 183–190 (2012).

[12] Nik Long N. M. A., Eshkuvatov Z. K. Hypersingular integral equation for multiple curved cracks problem in plane elasticity. International Journal of Solids and Structures. **46** (13), 2611–2617 (2009).

[13] Chen Y. Z., Hasebe N. Stress-intensity factors for curved circular crack in bonded dissimilar materials. Theoretical and Applied Fracture Mechanics. **17** (3), 189–196 (1992).

[14] Hamzah K. B., Nik Long N. M. A., Senu N., Eshkuvatov Z. K., Ilias M. R. Stress intensity factors for a crack in bonded dissimilar materials subjected to various stresses. Universal Journal of Mechanical Engineering. **7** (4), 172–182 (2019).

[15] Mayrhofer K., Fischer F. D. Derivation of a new analytical solution for a general two-dimensional finite-part integral applicable in fracture mechanics. International Journal for Numerical Method in Engineering. **33** (5), 1027–1047 (1992).

[16] Monegato G. Numerical evaluation of hypersingular integrals. Journal of Computational and Applied Mathematics. **50** (1–3), 9–31 (1994).

[17] Mason T. C., Handscomb D. C. Chebyshev Polynomials. Chapman and Hall/CR (2003).

[18] Kythe P. K., Schaferkotter M. R. Handbook of Computational Methods for Integration. Chapman and Hall/CRC (2004).

[19] Isida M., Noguchi H. Arbitrary array of cracks in bonded half planes subjected to various loadings. Engineering Fracture Mechanics. **46** (3), 365–380 (1993).

Виведення гіперсингулярних інтегральних рівнянь для термоелектричних зв'язаних матеріалів із тріщиною, паралельною межі поділу

Мохд Нордін М. Х. І.[1], Хамза К. Б.[2,3], Хашіе Н.С.[2,3], Вайні І.[2,3], Зайнал Н. А.[2,3], Саєд Нордін С. К.[2,3]

[1] *Факультет Кеджурутераан Пембуатан, Технічний університет Малайзії, Малакка, Ханг Туах Джая, 76100 Дуріан Тунгал, Малакка, Малайзія*
[2] *Технологічний факультет Кеджурутераан Механікал і Пембуатан, Технічний університет Малайзії, Малакка, Ханг Туах Джая, 76100 Дуріан Тунгал, Малакка, Малайзія*
[3] *Дослідницька група прогнозування та аналізу інженерних технологій (FETA), Технічний університет Малайзії, Мелака, Ханг Туах Джая, 76100 Дуріан Тунгал, Малакка, Малайзія*

У цій статті інтенсивно досліджується виведення гіперсингулярних інтегральних рівнянь (HSIE) для термоелектричних пов'язаних матеріалів (TEBM), що мають тріщину, паралельну межі розділу, що піддається напруженню зсуву в площині τ_{xy}^{∞}. Як правило, коефіцієнти інтенсивності напруження (SIF) розраховувалися за допомогою HSIE за допомогою модифікованої функції змінної комплексного напруження (MCSVF) й умов неперервності результуючої електричної сили та електричної функції зміщення. Невідома функція зміщення відкриття тріщини (COD), густина електричного струму та навантаження потоку енергії відображаються у функції сингулярності квадратного кореня з використанням методу координат кривої довжини як правого члена. Ця невідома функція потім використовується для обчислення безрозмірних SIF, щоб визначити поведінку стійкості TEBM із тріщиною, паралельною межі поділу, що піддається напруженню зсуву в площині τ_{xy}^{∞}. Наведено чисельні результати безрозмірних SIF у всіх вершинах тріщин. Отримані результати повністю узгоджуються з результатами попередніх робіт. Спостерігається, що безрозмірні SIF у вершинах тріщин залежать від співвідношення пружних констант, геометрії тріщин, електропровідності та коефіцієнтів теплового розширення.

Ключові слова: *термоелектричний; скріплені матеріали; поодинока тріщина; гіперсингулярні інтегральні рівняння; коефіцієнти інтенсивності напруженості.*